SLAC-PUB-12342

X-ray free-electron lasers

J Feldhaus[1], **J Arthur**[2] **and J B Hastings**[2]

[1] Deutsches Elektronen-Synchrotron DESY, D-22603 Hamburg, Germany
[2] Stanford Linear Accelerator Center, Stanford, CA 94309, USA

Abstract

In a free-electron laser (FEL) the lasing medium is a high-energy beam of electrons flying with relativistic speed through a periodic magnetic field. The interaction between the synchrotron radiation that is produced and the electrons in the beam induces a periodic bunching of the electrons, greatly increasing the intensity of radiation produced at a particular wavelength. Depending only on a phase match between the electron energy and the magnetic period, the wavelength of the FEL radiation can be continuously tuned within a wide spectral range. The FEL concept can be adapted to produce radiation wavelengths from millimetres to Ångstroms, and can in principle produce hard x-ray beams with unprecedented peak brightness, exceeding that of the brightest synchrotron source by ten orders of magnitude or more. This paper focuses on short-wavelength FELs. It reviews the physics and characteristic properties of single-pass FELs, as well as current technical developments aiming for fully coherent x-ray radiation pulses with pulse durations in the 100 fs to 100 as range. First experimental results at wavelengths around 100 nm and examples of scientific applications planned on the new, emerging x-ray FEL facilities are presented.

(Some figures in this article are in colour only in the electronic version)

1. Introduction

Basic physical principles tell us that small building blocks of matter, such as atoms, molecules, and nano-sized man-made structures, are able to very rapidly change their structure and properties in time: smaller is generally faster, as illustrated in figure 1. Exploration of the physics, chemistry and biology of the nanoworld therefore naturally demands experimental techniques and tools that can image sub-nanometre structure with sub-picosecond time resolution. Conventional lasers offer the required time resolution, but they cannot directly resolve the structures of atoms, molecules and the smallest man-made objects. On the other hand, today's synchrotron x-ray sources can be used to image the nanoworld, either by direct real-space imaging methods or by diffraction, but their time resolution is limited. The potential

Submitted to Journal of Physics B: Atomic, Molecular and Optical Physics

Work supported in part by the US Department of Energy contract DE-AC02-76SF00515

of providing the sub-picosecond pulse length of a conventional laser at the x-ray wavelength of a synchrotron radiation source is promised by the development of a new type of radiation source known as an x-ray free-electron laser (XFEL).

The free-electron laser (FEL) is in a sense an extension of the undulator radiation source that has proven so useful to the synchrotron community. An undulator is a periodic magnet array that imposes a periodic deflection on a relativistic electron beam. Interference effects enhance the probability of each electron emitting radiation at wavelengths selected by a phase match between the electron energy and the undulator period. Ordinarily, these interference effects apply independently to the radiation probability for each electron, with no inter-electron effects. However, with a very long undulator and a carefully prepared electron beam, an effect arises that is known as the FEL instability. It introduces correlations between the electrons, and opens the possibility of greatly enhanced peak x-ray brightness. This instability produces exponential growth of the intensity of the emitted radiation at a particular wavelength. The radiation field that initiates the instability can be either the spontaneous undulator radiation or an external seed field. In the case of FEL action arising from spontaneous radiation, the process is called self-amplified spontaneous emission (SASE). If an external seed is used then the FEL is referred to as an FEL amplifier.

Since the 1960s, research on the generation of short-wavelength coherent radiation has been concentrated mainly in the direction of atomic and molecular lasers, and optical resonators. While extremely successful in the infrared, visible and ultraviolet, these lasers have limited tunability, and this line of development has limitations at shorter wavelengths [1]. Short wavelengths can be produced by utilizing the nonlinear response of a material to up-convert visible laser light. For example, a gas target illuminated by an intense pulse of visible light can produce a series of high harmonics extending into the soft x-ray regime [2]. However, such processes are very inefficient. As electron beam techniques have become more advanced, the FEL has become a viable alternative to a conventional laser, especially for applications involving extreme tunability or high intensity at very short wavelengths.

Both conventional lasers and FELs rely on concepts first published by Einstein in 1905. But whereas conventional lasers have their scientific root in Einstein's paper on the photoelectric effect and the quantization of light [3], free electron lasers grow from a different source: Einstein's paper on special relativity [4]. The FEL process is essentially classical (see below), but it is intimately related to the relativistic transformations for fast-moving bodies and electromagnetic fields.

The FEL is the result of many years of theoretical and experimental work on the generation of radiation from relativistic electron beams. Theoretical work on FELs was done in the 1960s and 1970s by Palmer [5], Robinson [6] and Csonka [7]. In 1971, Madey [8] re-analysed the possibility of exchanging energy between free electrons and electromagnetic radiation in the small-gain regime, using a quantum-theoretical approach. This was followed by successful experimental demonstration of an FEL amplifier [9], and an FEL oscillator [10] at 10 μm wavelength by Madey and collaborators.

This initial work was based on the small-gain regime of FEL amplification, requiring multiple passes of an electron pulse through an optical cavity to build up the FEL field. The idea of using the FEL collective instability to produce infrared radiation using a single-pass amplifier starting from noise was first proposed by Kondratenko and Saldin in 1980 [11]. Murphy and Pellegrini in 1985 [12] proposed use of the FEL instability in a single-pass amplifier starting from noise for soft x-rays. The choice of a single-pass device for the x-ray region is motivated by the fact that optical cavities have large losses and are difficult to build at short wavelengths.

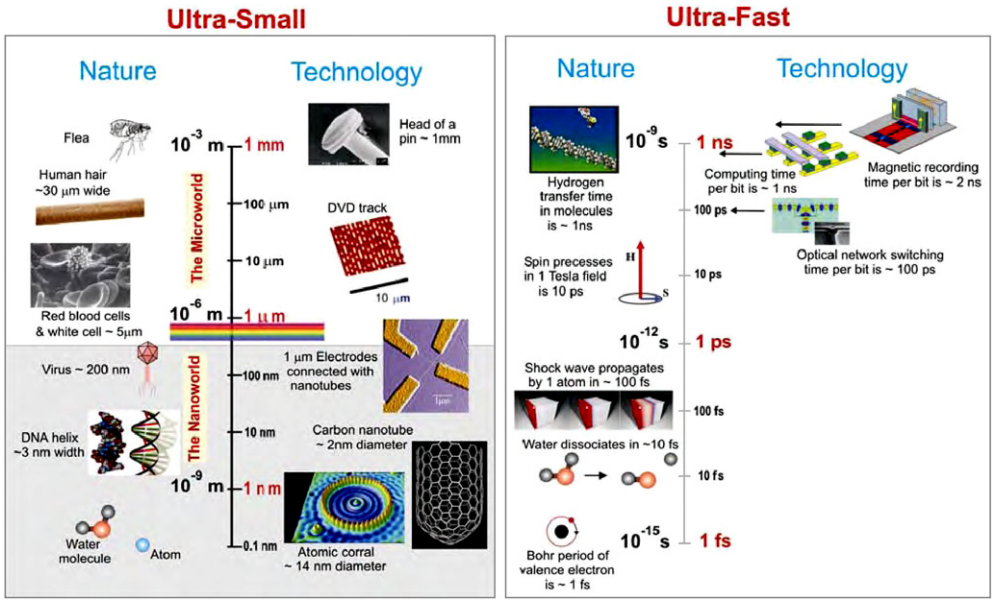

Figure 1. X-rays have opened the ultra-small world. XFELs will open the ultra-small and ultra-fast worlds. Graphic courtesy of J Stöhr.

These ideas motivated the investigation of the scaling laws [13] for a single-pass FEL starting from noise to reach the 0.1 nm wavelength regime. The analysis showed that the gain of a SASE-FEL depends on wavelength, and that to reach the soft or hard x-ray region one needs an electron beam that is very dense in six-dimensional phase-space, a condition which until recently was difficult to satisfy.

The development of radio frequency photocathode electron guns [14], and the emittance compensation method [15, 16] changed this situation. At the same time, work on linear colliders demonstrated that it is possible to accelerate and time-compress electron beams without spoiling their brightness [17–20]. This has recently been confirmed experimentally at the sub-picosecond pulse source at SLAC, where 30 kA peak currents are achieved from 80 fs, 3 nC electron bunches accelerated to 28 GeV [21]. These developments have led to major FEL projects in both Germany and the US, which should soon produce SASE-FEL radiation down to about 0.1 nm, with peak power of tens of GW, pulse length of about 100 fs (FWHM) or shorter, full transverse coherence and peak brightness about ten orders of magnitude larger than that of existing synchrotron radiation sources.

2. The FEL process

The gain medium of a FEL is a relativistic electron beam moving through the periodic magnetic field of an undulator. In its simplest form an FEL is just a very long undulator, typically five to ten times longer than those used as synchrotron radiation sources [22]. When the quality of the electron beam in terms of charge density, emittance and energy spread is sufficiently high, the interaction between the electrons oscillating in the undulator magnetic field, and the synchrotron radiation that they spontaneously produce, leads to an instability of the electron bunch. Its density becomes modulated periodically in the longitudinal direction with a period length equal to the wavelength of the undulator fundamental radiation. The

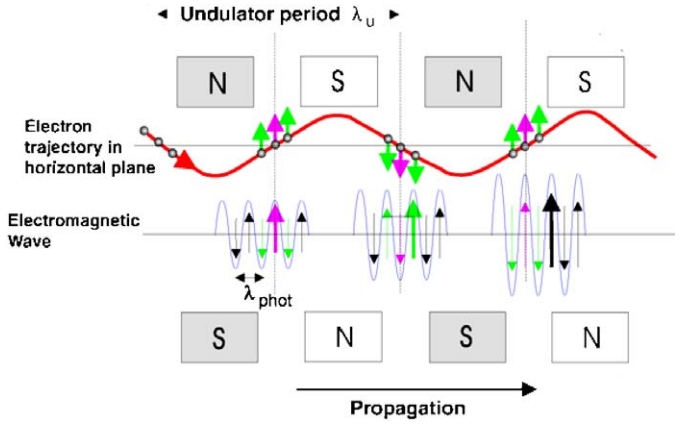

Figure 2. The electron orbit in a periodic undulator field (undulator period λ_u). Three electrons and the field of an electromagnetic wave (wavelength λ) are shown at three positions along the undulator. While the electrons move through a full oscillation period λ_u, the electromagnetic wave propagates by λ_u plus one wavelength λ. The transverse movement of each electron has a constant phase with respect to the electromagnetic field.

bunched electrons, due to their spatial grouping, proceed to radiate in phase with each other, in contrast to conventional undulators where the electrons radiate independently. The intensity gain of a FEL is therefore of the order of the number of particles involved and can be as high as 10^8.

Initially, the physics of the free-electron laser was described in the quantum mechanical picture as stimulated emission of bremsstrahlung in a periodic magnetic field [8]. However, the classical theory is more instructive and is, in fact, completely adequate since the photon energy of the FEL is orders of magnitude smaller than the electron energy bandwidth involved. Therefore, virtually all theoretical developments and numerical simulations in recent years have been based on a classical treatment (see, e.g., [23]). The basic gain mechanism of an FEL can be derived from the equations of motion in the presence of a nearly constant radiation field, i.e. in the low-gain regime. The electrons are deflected periodically by the magnetic field and can therefore exchange energy with a superimposed radiation field $\vec{E}$:

$$\frac{\mathrm{d}E_\mathrm{e}}{\mathrm{d}t} = -e\vec{v}_\mathrm{e} \cdot \vec{E}. \tag{1}$$

E_e is the electron energy and $\vec{v}_\mathrm{e}$ is the electron velocity, which has a small transverse component in the direction of $\vec{E}$ due to the oscillation. The energy exchange is optimum for wavelengths close to the on-axis undulator resonance

$$\lambda = \frac{\lambda_\mathrm{u}}{2\gamma^2}\left(1 + \frac{K^2}{2}\right) \tag{2}$$

where $\gamma = E_\mathrm{e}/m_0c^2$ is the electron energy in units of the electron rest mass, λ_u is the undulator period and K is the undulator parameter which is proportional to the magnetic field (see [22]). For the resonance wavelength λ the path length difference between radiation and electrons over one magnet period λ_u is λ, and the transverse oscillation of each electron is perfectly synchronous with the radiation field (see figure 2). Exactly on resonance there are as many particles that gain energy as particles that lose energy, such that the net gain is zero. Slightly above resonance, however, this mechanism leads to a net energy transfer from the electron beam to the radiation field.

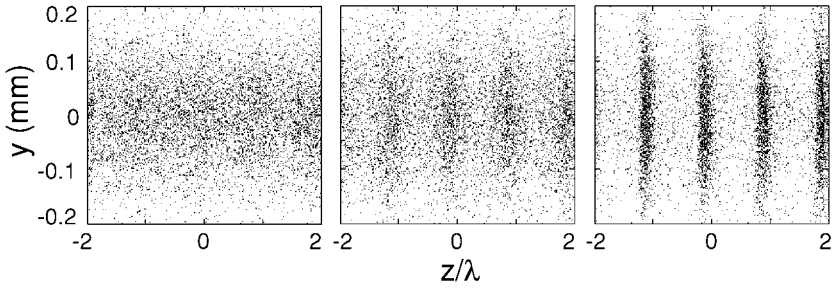

Figure 3. Simulation of the density modulation of the electron beam as it develops along the undulator. The electron density is represented by the density of the dots (left: at the undulator entrance, middle: in the middle of the exponential growth regime, right: at the undulator exit, i.e. for saturation).

Depending on its phase with respect to the electromagnetic field, an electron is accelerated or decelerated by the field on its way through the undulator, leading to a periodic velocity modulation of the electrons along the beam with a period equal to the wavelength λ of the superimposed radiation field. This velocity modulation transforms eventually into a periodic longitudinal density modulation (figure 3) such that more and more electrons radiate coherently. This, in turn, enhances the interaction with the electron beam and causes an exponential intensity growth up to a saturation level where maximum bunching is reached.

In the high-gain regime of the FEL the simple theoretical approach indicated above is no longer sufficient. Also, the electrostatic forces between the electrons have to be taken into account. It is therefore necessary to solve the equations of motion together with Maxwell's equations in a self-consistent way (see, e.g., [23]). This is possible by means of three-dimensional time-dependent numerical simulation codes. Several such codes have been developed over the last few years (see, e.g., [24, 25]). They allow one to study the influence of all relevant electron beam parameters such as charge density, emittance, energy spread, the axial and transverse profiles of the electron bunch, and the finite pulse duration, and may even include the interaction with the walls of the vacuum chamber, and undulator field errors and misalignment. These codes have provided the basis for stringent tests of existing FELs and for optimizing the parameters of future facilities.

After the first demonstration of an FEL amplifier which was seeded by a CO_2 laser at 10.6 μm wavelength [9], the FEL gain process has been employed in different ways to build free-electron lasers. Many FEL oscillators have been constructed which work in the infrared and visible region, with wavelengths from several hundred μm to $<$200 nm, using optical cavities and suitable electron bunch timing in the linear accelerator or storage ring (see figure 4).

It is difficult to push the fundamental wavelength of an FEL oscillator far below 200 nm because the intense, collimated UV radiation destroys the mirror surfaces (high reflectivity mirrors are not available for very short wavelengths). Therefore it has been proposed to generate short-wavelength FEL radiation down to the Ångstrom (0.1 nm) region in a single pass through a very long undulator, simply amplifying the spontaneous radiation emitted near the entrance to the undulator. Theoretical work on this concept of self-modulation of a relativistic electron beam, which has come to be called self-amplified spontaneous emission (SASE), started in the late 1970s [11, 26]. Since a FEL based on SASE requires very high electron beam quality, the technical realization at short wavelengths has become feasible only recently due to the advances made in the quest for a new generation of linear colliders

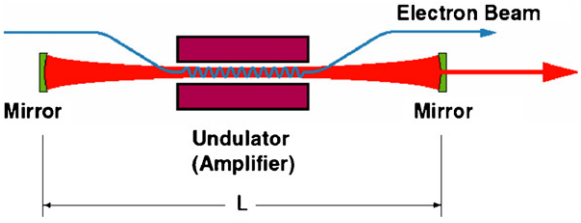

Figure 4. Principle layout of a FEL oscillator. The mirrors are not needed for a single-pass FEL operating in the SASE mode but the undulator must be sufficiently long to reach saturation in a single pass.

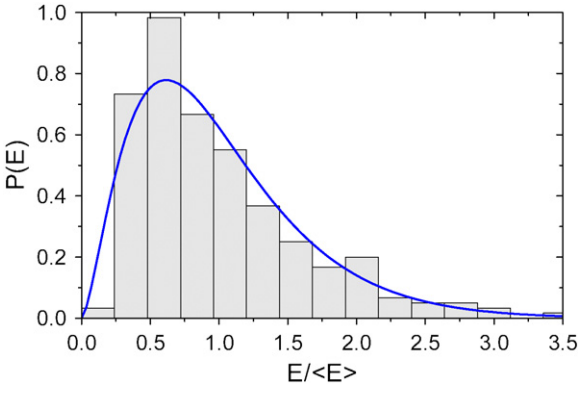

Figure 5. Probability distribution of the radiation pulse energy E at 95 nm wavelength measured in the linear gain regime of the VUV-FEL at DESY.

for particle physics. Several recent experiments in different laboratories have successfully demonstrated the high gain of SASE at ever shorter wavelengths [27–30], providing the basis for a new generation of short-wavelength radiation sources. The first user facility for VUV and soft x-ray radiation based on a SASE FEL will become operational at DESY, in Hamburg, Germany, in 2005 [31]. The LCLS project at SLAC [32], now under construction, will provide hard x-rays down to 0.15 nm wavelength by 2009, and a large European XFEL facility at DESY [33] for wavelengths below 0.1 nm is expected to follow a few years later.

3. The characteristics of SASE FEL radiation

The properties of the radiation generated by a SASE FEL are closely related to its start-up from noise. Due to the shot noise in the electron beam the amplitudes and phases of the radiation produced in the entrance of the undulator are random in space and time. The radiation properties are those of completely chaotic polarized radiation known from statistical optics. The amplification in the FEL does not change these properties except in the saturation regime. The statistical properties of SASE FEL radiation have been studied theoretically by different authors, both in the linear and nonlinear regime (e.g. [34, 35]). They have subsequently been verified experimentally at the TESLA test facility (TTF) at DESY for VUV wavelengths around 100 nm [36, 37]. Figure 5 shows the probability distribution $P(E)$ of the radiation pulse energy E, measured at 95 nm wavelength in the linear gain regime at an active undulator

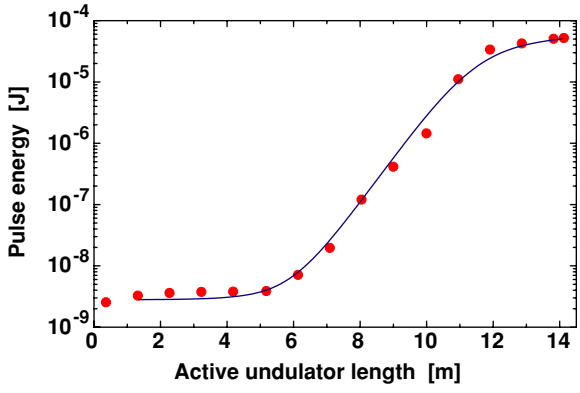

Figure 6. Gain curve of the VUV-FEL at the TESLA test facility at DESY measured at a wavelength of 98 nm [26, 32]. The dots are the average energy in the radiation pulse measured as a function of the active undulator length. The solid curve is a numerical simulation.

length of 9 m. As predicted by theory, the experimental distribution is in good agreement with the gamma distribution

$$P(E) = \frac{M^{\mathrm{M}}}{\Gamma(M)} \left(\frac{E}{\langle E \rangle}\right)^{\mathrm{M}-1} \frac{1}{\langle E \rangle} \exp\left(-M \frac{E}{\langle E \rangle}\right) \tag{3}$$

with $M = 1/\sigma_{\mathrm{E}}^2 \cdot \sigma_{\mathrm{E}}$ is the standard deviation of the radiation pulse energy. For the case of figure 5 the best fit was obtained for $M = 2.6$.

The parameter M can be interpreted as the number of modes contributing to the radiation pulse. Together with the gain length $L_{\mathrm{g}} = 67 \pm 5\,\mathrm{cm}$ derived from the measured gain curve shown in figure 6, it is possible to estimate the radiation pulse duration $\tau_{\mathrm{rad}} \simeq M L_{\mathrm{c}}/c$ where $L_{\mathrm{c}} \simeq 2\lambda L_{\mathrm{g}}/\lambda_{\mathrm{u}} \simeq 5\,\mu\mathrm{m}$ is the coherence (or cooperation) length. The result is a pulse duration $\tau_{\mathrm{rad}} \simeq 50\,\mathrm{fs}$. For a typical pulse energy of 50 μJ this corresponds to a peak radiation power of $\sim$1 GW. This is a typical value for the VUV radiation from a SASE FEL at saturation. At x-ray wavelengths around 0.1 nm simulations predict peak power levels in the 10 to 100 GW range. In order to extract maximum power from the electron beam, tapered undulators would have to be used in order to stay on resonance [38].

The pulse duration can also be estimated from the spectral distribution shown in figure 7. In the time domain the radiation is emitted in short bursts with length L_{c}, with random phase relationships between the bursts. The Fourier transform of such a spikey pulse results in narrow spikes in the spectral domain whose widths $\Delta\omega$ are given by the pulse duration: $\Delta\omega \simeq 2\pi/\tau_{\mathrm{rad}}$. The upper panel of figure 7 shows the spectral distribution of a single radiation pulse measured at maximum electron bunch compression, resulting in an average number of $M = 2.6$ modes. The pulse duration $\tau_{\mathrm{rad}} \simeq 50\,\mathrm{fs}$ derived from the spectral line width is consistent with that estimated from the statistical intensity fluctuations. The lower panel of figure 7 shows the spectral distribution of a single radiation pulse for a somewhat weaker electron bunch compression. The pulse duration is now $\tau_{\mathrm{rad}} \simeq 100\,\mathrm{fs}$ which is reflected in the narrower line widths and the larger number of modes, $M = 6$. The average spectral envelope $\Delta\omega_{\mathrm{avg}}$ is not much changed since it is determined by the coherence length. However, the measured value of $\Delta\omega_{\mathrm{avg}}$ is approximately twice as large as that estimated from the gain length, and the profile is also distinctly asymmetric for the shortest pulses. More recent FEL simulations are in full agreement with these results [39]. They use a more realistic electron distribution based on the so-called start-to-end simulations of the electron bunch from the

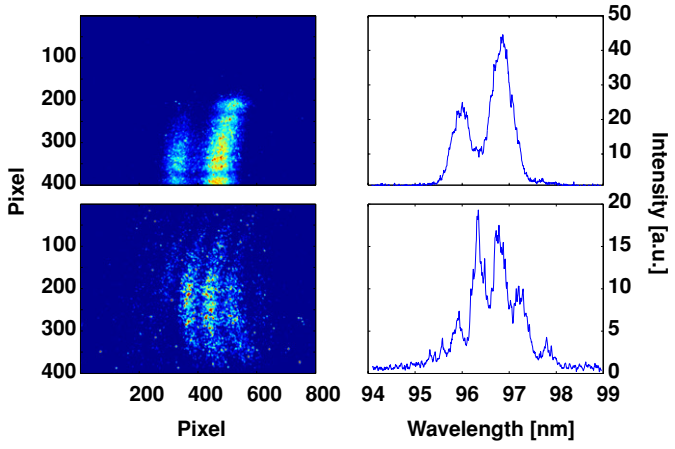

Figure 7. Spectra of single FEL pulses. The CCD image of the horizontally dispersed FEL radiation is shown in a false colour code on the left. The spectral profiles scanned along the horizontal centre line of the CCD image are shown on the right hand. The upper spectrum is that of a short pulse (∼50 fs) with an average of $M = 2.6$ modes, the lower spectrum belongs to a longer pulse (∼100 fs) with $M = 6$.

electron gun to the entrance of the undulator, revealing strong space charge effects which result in a large correlated energy spread.

While the temporal coherence of a radiation pulse generated by a SASE FEL is only partial, the spatial coherence can be very high. Although a large number of transverse radiation modes are excited in the entrance section of the undulator, the fundamental mode dominates when saturation is reached because it overlaps the electron beam more than other modes and therefore experiences the highest amplification. The high degree of spatial coherence can be seen in the diffraction pattern of a double slit behind the VUV-FEL measured at a wavelength of 95 nm (figure 8). A series of diffraction patterns taken at different active undulator lengths confirmed that the degree of spatial coherence increases until saturation is reached; in the deep saturation regime, however, it decreases again slowly because other modes catch up [40].

4. Technical developments to improve the temporal coherence

The statistical properties of SASE FEL radiation discussed in the previous section can be quite unfavourable for certain applications. For example, spectroscopic techniques are frequently used in the VUV and soft x-ray (XUV) spectral range, therefore the spectral distribution of each radiation pulse needs to be controlled, or at least monitored in a non-destructive way. For time-resolved experiments or studies of nonlinear effects—both key areas of research for future XUV FELs—it is also crucial to know the temporal structure. It is therefore essential to develop suitable online diagnostics in order to sort and interpret the data.

The pulse energy can be monitored by measuring the ionization current of a rare gas with known absorption cross section at low pressure. The method is well known and has been adapted to short, intense radiation pulses with high repetition rate. It was successfully tested at TTF [41] and will be used routinely at the upcoming VUV-FEL user facility at DESY. The online, pulse-resolved and non-destructive measurement of the spectral distribution appears to be technically feasible [42], and the development of a suitable spectrometer integrated in the radiation beamlines of the VUV-FEL is underway. The measurement of the temporal structure

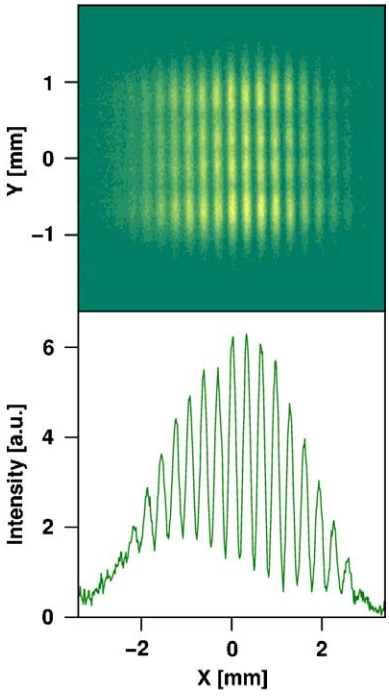

Figure 8. Diffraction pattern of two parallel slits illuminated with 95 nm FEL radiation, illustrating the high degree of transverse coherence. Each slit is 2 mm high and 0.2 mm wide; they are 1 mm apart. The slits are located 12 m behind the exit of the undulator. The image was recorded by a gated CCD camera viewing a Ce:YAG fluorescent screen 3 m behind the slits. Several consecutive FEL pulses were accumulated. The lower part is a horizontal cut through the centre of the diffraction pattern.

of single radiation pulses with high resolution, however, is still in a very early, experimental stage, and it is not certain at the present time if this can ever be done routinely, online and with sufficient resolution.

It would be much more elegant if the FEL process could be controlled in such a way that Fourier-limited radiation pulses with adjustable duration could be produced. This is straightforward, in principle, if the FEL is used not in the SASE mode (where it amplifies the shot noise in the electron beam), but rather as an amplifier seeded by coherent radiation. Since seed pulses of sufficiently intense, coherent radiation are not now available at very short wavelengths, two different routes to achieve coherent seeding have been investigated.

One is to use an optical seed laser (or a higher harmonic generated in a nonlinear crystal or a gas) for the first stage of an FEL cascade making use of high-gain harmonic generation (HGHG). The schematic layout of a HGHG FEL is shown in figure 9. The first, short undulator, called the modulator, is tuned to the frequency of the coherent seed laser whose interaction with the electron beam introduces a small longitudinal energy modulation. The magnetic dispersion section converts this energy modulation into a density modulation. The second undulator, called the radiator, is tuned to the nth harmonic of the seed frequency. When the modulated electron beam passes the radiator, the radiation produced by the nth harmonic component is amplified to saturation. This concept was demonstrated in the mid-infrared by seeding with a CO_2 laser and generating the second harmonic in the radiator [43]. Later this scheme was employed to generate intense, coherent ultraviolet radiation at 266 nm wavelength

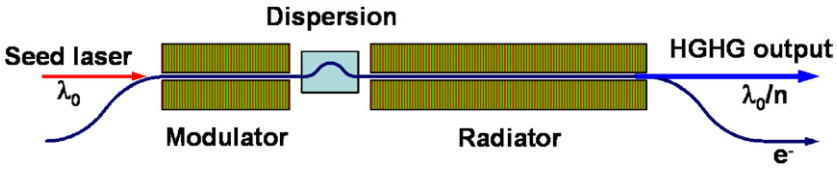

Figure 9. Principle layout of the high-gain harmonic generation (HGHG) scheme.

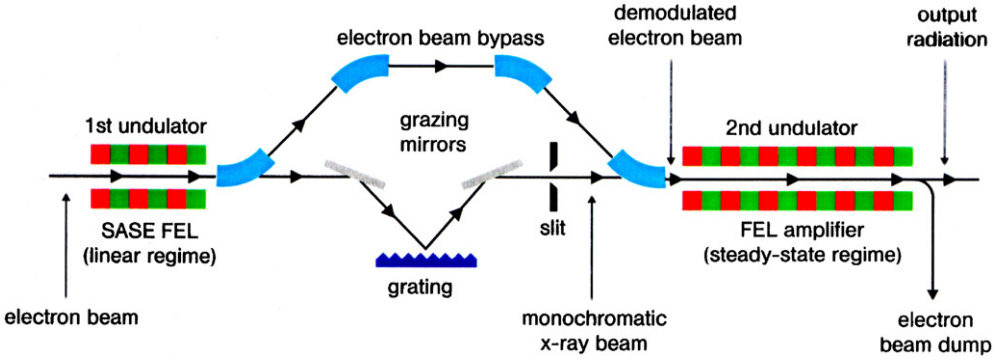

Figure 10. Schematic layout of a self-seeded FEL for XUV wavelengths.

as the third harmonic of 800 nm using a Ti:sapphire seed laser [44]. The radiation pulse energy at saturation was typically 100 μJ with a pulse duration of $\sim$0.6 ps. The third harmonic of the output radiation at 88 nm wavelength, still at the 1 μJ level, was successfully used for first experiments probing the superexcited-state dynamics of methyl fluoride [45].

HGHG can be used to generate radiation pulses with $<$20 fs duration, and in principle the HGHG FEL can be cascaded to reach still-shorter wavelengths. This concept is currently being discussed for the next generation of XUV and x-ray sources. However, simulations and theoretical investigations have shown that the beam quality will eventually be degraded by noise which is also amplified [46, 47]. At the present time it is not clear where the physical and technical limits are, therefore intensive research and development is ongoing.

The other possible route to a temporally coherent x-ray FEL is to produce the coherent seed radiation in a SASE FEL tuned to the same wavelength [48]. This concept, also called self-seeding, has the advantage that it is independent of any external radiation source (which must be very stable, continuously tunable, operate at short wavelengths, and must be precisely matched to the electron beam in space and time, synchronised to $<$100 fs). The schematic layout of a self-seeded FEL for the XUV region is shown in figure 10. The first undulator, a short SASE FEL operating in the linear gain regime, produces radiation pulses with the characteristic features of SASE (figure 11, left panel) at a power level approximately three orders of magnitude below saturation in order not to spoil the electron beam quality. The electron beam is then sent through a magnetic chicane which is designed such that it destroys the density modulation introduced in the first undulator and delays the electron beam by the same amount as the radiation pulse. The radiation pulse is spectrally filtered by a narrow-band grating monochromator which stretches the pulse and provides a coherence length longer than the electron bunch length. This radiation is the seed for the second undulator which amplifies it to saturation.

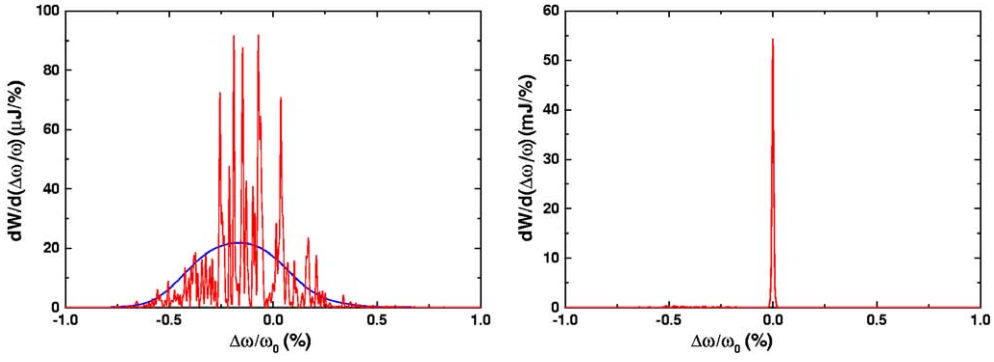

Figure 11. Spectral power distribution after the first (left) and the second undulator (right).

The output radiation exhibits a narrow spectral line with only a small background of spontaneous radiation (figure 11, right panel). The pulse energy is the same as that of a FEL operating in the SASE mode, thus the spectral brightness has increased by almost two orders of magnitude. Due to the saturation in the FEL amplifier, the intensity of the single-line output radiation is rather insensitive to the fluctuating input seed intensity, although now and then the shot noise dominates. The statistical properties have been carefully studied and the design parameters optimized [49]. The hardware components for a self-seeding mode of the VUV-FEL at DESY, covering a range of 6–60 nm wavelength, are currently under construction and will be installed and tested in the near future.

5. Generation of femtosecond and attosecond x-ray pulses

The x-ray pulses generated by the SASE FELs currently in operation or under construction are $\sim$100 fs long, owing to the compression schemes used for the electron beam. This is considerably longer than the lifetimes of electronic states accessible with nanometre and sub-nanometre radiation, which are in the few-femtosecond to sub-femtosecond (attosecond) range. Even some molecular vibrations can be as short as $\sim$10 fs. Therefore, a new range of scientific applications would be opened if the duration of the radiation pulses could be reduced by one to two orders of magnitude. This should be possible in principle, since the coherence time varies from several fs to a few hundred attoseconds for wavelengths between 10 nm and 0.1 nm. Several different strategies are being considered for generating ultra-short pulses.

The test experiments at TTF have shown that bunch compression to $<$100 fs is possible. Optimized bunch compression techniques might well reduce the pulse duration to the 10 fs range. Short-pulse XUV radiation with pulse durations down to $\sim$10 fs can be produced by cascaded HGHG FELs seeded by femtosecond optical laser pulses. Recently, several techniques have been proposed for achieving even shorter pulse durations. They rely on three different approaches: (i) selection of single radiation spikes employing the statistical properties of the radiation [50], (ii) use of energy-chirped electron bunches [51, 52] and (iii) local energy modulation of the electron beam by a strong optical laser pulse [38, 53–55].

Saldin *et al* [50] propose to start with a SASE FEL at 0.8 nm operating in the high-gain linear regime, and to generate 0.1 nm radiation by frequency multiplication in three successive steps. The nonlinear harmonic generation increases the intensity fluctuations drastically such that the single highest radiation spike in the 0.8 nm pulse dominates the distribution at the eighth harmonic at 0.1 nm. It is sufficient to set a threshold for the pulse energy to select single

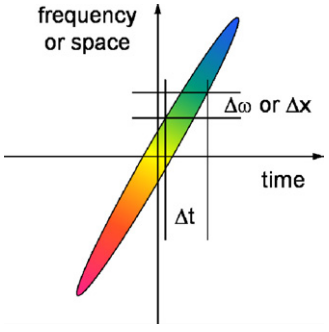

Figure 12. An energy-chirped bunch produces a frequency-chirped radiation pulse. A narrow-band monochromator or a slit in a dispersion section of the accelerator selects a short time slice.

radiation spikes with ∼0.5 fs duration. The higher the threshold, the higher is the contrast and the lower the probability for finding pulses that exceed the threshold. For example, a threshold set at twice the average pulse energy would result in a single-line contrast of 90% at an occurrence of 10%.

Energy-chirped electron bunches can be used in different ways to prepare fs x-ray pulses. The energy-chirped electron bunch generates a radiation pulse whose frequency varies as a function of position, i.e. time, along the pulse. The selection of a narrow frequency band then produces a pulse that is much shorter than the original one (see figure 12). Schroeder *et al* [51] propose to impose a strong energy chirp of 0.5% on the electron bunch. A narrow-band monochromator selects a short temporal pulse which is then amplified to saturation in a second undulator. The pulse duration is determined by the SASE bandwidth, the monochromator bandwidth and the frequency chirp [56]. Pulse durations around 10 fs seem to be realistic. Instead of selecting a narrow bandwidth in the frequency domain, Emma *et al* [52] propose to introduce a narrow slit, made of a thin carbon foil, in the bunch compressor chicane where the (only slightly) energy chirped electron bunch is dispersed in space. The thin carbon foil spoils the electron beam emittance so much that only the narrow part passing the slit supports the FEL process. Simulations show that ∼1 fs, saturated x-ray pulses at the 10 GW level could be generated at 0.15 nm wavelength.

The third approach makes use of intense optical laser pulses, which modulate the energy of the electron beam. If a very short optical pulse is used, with only a few cycles, and a carrier-envelope phase adjusted such that the peak electric field coincides with the envelope peak, a strong local energy modulation is imposed on the electron beam, larger than the FEL bandwidth. Therefore, the FEL undulator can be tuned such that it amplifies only within a small fraction of the optical cycle and produces ∼0.3 fs x-ray pulses [38, 53, 54]. This method can be modified by adding a magnetic dispersion section enhancing the electron density periodically at the frequency of the optical laser [55]. This enhances the SASE process periodically ('current-enhanced SASE'), leading to a sequence of narrow (∼0.2 fs) radiation spikes. The number of spikes depends on the length of the optical pulse and can in principle be reduced to a single spike.

6. Current status of x-ray FEL projects

The best source for the current status of FEL projects is http://sbfel3.ucsb.edu/www/vl_fel.html. There are many operating FELs in the few to 10s of micron wavelengths worldwide. The VUV

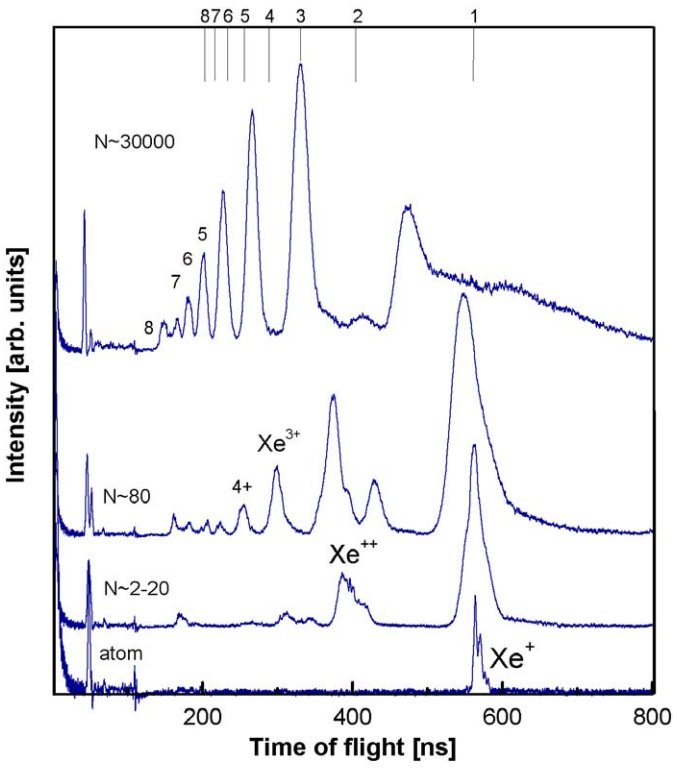

Figure 13. Time-of-flight spectra of the ionization products of Xe atoms and clusters after irradiation with 98 nm FEL radiation at an average power density of 2×10^{13} W cm^{-2}. N is the average number of atoms in the cluster.

FEL at DESY is about to become operational with a goal of reaching 6 nm in the not too distant future. There are in addition to the LCLS at SLAC (under construction) and the European XFEL in Hamburg (in advanced design), several other FEL proposals pointed toward reaching 1 nm or below. This is an emerging field and there is growing excitement worldwide for the development of these unique light sources.

7. First experimental results at VUV wavelengths

The GW level VUV pulses from the SASE FEL at the TTF at DESY have been used for two exploratory experiments on gases and solids demonstrating the unique properties of the new radiation source. For both experiments the radiation was focused by an ellipsoidal mirror to approximately 20 μm diameter with power densities up to more than 10^{13} W cm^{-2}. The sample position could be moved along the FEL beam in order to vary the fluence by some three orders of magnitude. Figure 13 shows time-of-flight (TOF) mass spectra of the ionization products of Xe atoms and clusters after irradiation with 98 nm FEL radiation at an average power density of 2×10^{13} W cm^{-2} [57]. At this power level every single Xe atom in the beam is ionized after a few femtoseconds since the photon energy (12.7 eV) is just above the photo-ionization potential of Xe (12.1 eV) and the ionization cross section is approximately 50 Mb (1 Mb $= 10^{-18}$ cm^2).

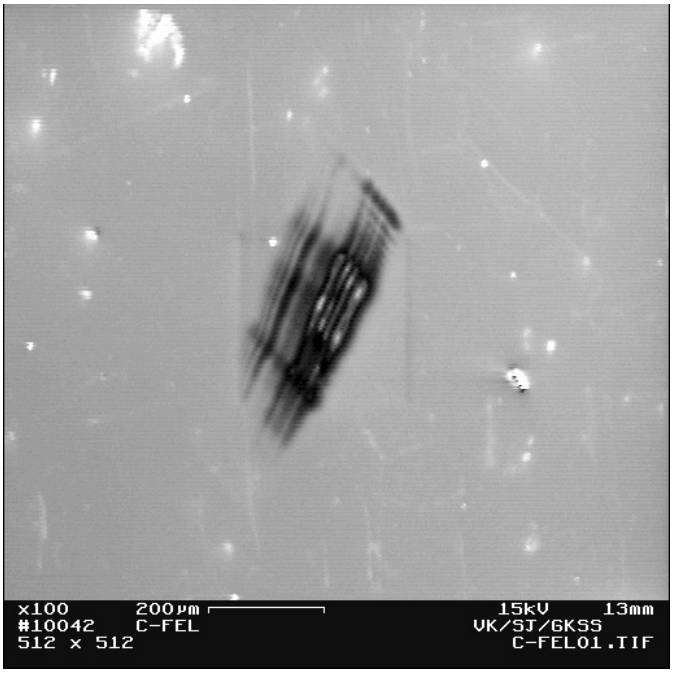

Figure 14. Scanning electron microscope image of a carbon coated mirror irradiated by the TTF FEL beam with 98 nm wavelength at a fluence of ∼0.2 J cm^{-2}. The spot diameter is approximately 0.2 mm. The black lines indicate regions of high intensity where material is ablated.

For atomic Xe, only singly charged Xe^+ ions are observed; multiple ionization is still negligible (lower curve in figure 13). The splitting of the Xe^+ line is caused by different isotopes. When Xe clusters are exposed to the same power density, highly charged ions up to X^{8+} are observed. The larger the clusters, the higher the charge states and the higher their initial kinetic energy as indicated by the shift of the lines. While Xe atoms absorb only a single photon, the absorption in clusters is strongly enhanced. At 7×10^{13} W cm^{-2} and 98 nm wavelength, each atom in large clusters absorbs up to 30 photons, i.e. ∼400 eV. Subsequently, the clusters completely disintegrate in a Coulomb explosion. The reasons for the increased absorption and the development of the unexpectedly high charge states have been discussed in several publications (see, e.g., [58]). Obviously, multiple ionization of atoms in a cluster is facilitated by the influence of the neighbouring atoms. The nanoplasma formed by the first part of the radiation pulse is then further heated by inverse bremsstrahlung processes. The development of high-charge states is related to the finite cluster size and the dynamics of the explosion of the nanoplasma.

It should be mentioned that the results for the ionization of atomic Xe shown in figure 13 were different when the measurements were repeated a few weeks later at slightly different FEL beam conditions. In the later measurement, Xe charge states up to Xe^{4+} were observed at the same power density of 2×10^{13} W cm^{-2} which had only produced Xe^+ ions earlier [59]. The reason could be a different temporal structure of the radiation pulse, caused by different settings of the electron bunch compressor (see also figure 7).

In the second experiment the interaction of the intense VUV radiation pulses with different solids was investigated [60, 61]. A range of different samples, including Si, SiO_2, Au, PMMA and thin Au and C coatings on Si wafers, was irradiated with fluences up to >1 J cm^{-2}. Figure 14 shows a damaged amorphous carbon coating on a silicon wafer after irradiation

with 98 nm FEL pulses. Carbon coatings have been investigated because they are the preferred mirror material for VUV and soft x-ray FEL radiation below the carbon K-edge [62]. The ions leaving the surface were detected by a time-of-flight spectrometer. As in the cluster experiments, multiply charged ions with high kinetic energies were detected at high fluences. For most samples the threshold values for the emission of ions were on the order of 50 mJ cm^{-2}. A careful post-mortem analysis of the irradiated samples using atomic force microscopy (AFM), Nomarski microscopy and Raman spectroscopy revealed lower damage thresholds. The first change is seen as a modification of the refractive index, which occurs already at fluences between 5 mJ cm^{-2} (for Si) and 30 mJ cm^{-2} (for SiO_2). The thresholds for surface deformation detected by AFM are between 10 mJ cm^{-2} (for PMMA and a 15 nm Au coating on Si) and 40 mJ cm^{-2} (for Si). The ablation behaviour of conducting or semiconducting materials and insulators was found to be distinctly different in terms of crater morphology and kinetic energy of the ejected ions. The low damage thresholds seem to be acceptable for the optics layout of the new VUV-FEL user facility at DESY: a worst case estimate for 6 nm wavelength and 1 mJ pulse energy results in <0.3 mJ cm^{-2} absorbed by the carbon mirror coating.

8. Future scientific applications

The evolution of scientific understanding typically begins with statics and evolves to dynamics. In studying natural processes, it is usually easier to explore structures than functions. So it is in the nanoworld, too. X-rays with Ångstrom wavelengths have provided detailed structures of ever-more-complex systems, with resolution on the atomic scale. Crystallography can now study proteins with tens of thousands of atoms and determine the average, static atomic positions with few-Ångstrom resolution. This has proved immensely useful. However, a more sophisticated understanding of nano*structure* raises more questions about nano*dynamics*. To study the dynamics of nanosystems, the most common tools today are conventional lasers, which can routinely provide pulse lengths on the order of tens of femtoseconds, and under special circumstances less than 1 fs [63]. These fast pulses are needed to study the short-range motions of atoms undergoing chemical reactions, phase transitions in solids and fast dynamics in biological systems. Unfortunately, the laser wavelengths are hundreds of times longer than the interatomic spacing, so that directly observing atomic positions (as one could do with x-rays) is not possible with lasers. The laser measurements rely on the inference of the atomic motions through spectroscopic measurements, indirectly observing position changes through their effects on atomic and molecular energy levels. This indirect approach becomes very difficult for all but the simplest systems. The XFEL will allow direct observation of atomic positions, with femtosecond time resolution, and should become the basic tool to study atomic scale dynamics on the natural time scales of interest in materials science, chemistry and biology. More broadly, this new source of x-rays will enable the study of transient structures in molecules, liquids and solids either as a probe or as a pump to create these states. The range of these applications has been elucidated in the first experiments document for the LCLS [64] and the technical design report for the TESLA XFEL [33]. In the paragraphs below we will outline two of these areas: laser-pump-x-ray-probe studies of chemical dynamics, and near-atomic-resolution diffraction imaging of single nanoscale objects. These examples give some idea of the scientific breadth to be spanned by the XFEL research, and begin to answer questions like ‘can we see how matter forms and changes?,’ ‘can we image single macromolecules?’, and ‘can we produce a movie of a chemical reaction with atomic resolution?’.

8.1. Structural dynamics in chemistry and molecular biology

The fundamental events of chemistry and molecular biology occur on the distance and time scales governed by chemical bond lengths and vibrational periods. These chemical bond properties make x-ray science (with Ångstrom spatial resolution) and ultrafast laser science (with femtosecond temporal resolution) the optimal experimental tools today for molecular-scale investigations of chemical phenomena. Conventional x-ray scattering can determine the static structures of molecules, and femtosecond optical probes can observe the temporal evolution of excited molecules (by observing the temporal evolution of absorption spectra). The successful combination of laser and x-ray probes in the femtosecond regime has been limited by the inherently long pulse duration of a synchrotron (typically 100 picoseconds) and the extremely low x-ray flux of specialized ultrafast x-ray sources such as laser plasma sources. XFELs overcome both of these limitations. These ultrafast hard x-ray sources, when combined with ultrafast optical lasers, will provide a unique opportunity to observe chemical and biological phenomena with unprecedented temporal and spatial resolution.

The need to develop a detailed molecular-scale understanding of chemical reactivity motivates the ultrafast experimental studies of chemical dynamics. Much of our understanding of chemical reaction dynamics has been acquired with ultrafast optical spectroscopy [65–71]. Of particular significance in these time-resolved studies has been the investigation of photodissociation and recombination [66, 70–80], photoisomerization [69, 81–92] and photoinitiated electron transfer reactions [67, 68, 93–96] at surfaces and in liquids, glasses, solids and proteins. While these extensive investigations have led to a wealth of information regarding chemical reaction dynamics in the condensed phase, critical aspects of the dynamics and the influence of the environment on chemical and biological reactions have yet to be fully characterized experimentally.

Diffraction methods that have atomic-scale resolution are unique in their ability to correlate length and time scales with greater certainty than can strictly optical measurements, in most systems. The first attempts at this in the gas phase have used electron diffraction [97]. There, time resolution is limited to the picosecond scale by space charge effects in the probe electron beam. The XFEL does not have this limitation. Both the temporal and the per-pulse intensity provide the opportunity to identify the reaction coordinate and reaction intermediates, and construct reaction mechanisms with unprecedented spatial precision and temporal resolution.

Given sufficient photo-excitation yields, crystallography provides the most powerful tool for measuring the well-ordered structures of excited molecules. This approach has been successfully applied in a variety of time-resolved crystallography measurements [98–104] and will certainly be a useful approach for experiments at XFELs. Crystallography does not, however, fully describe the influence of photoexcitation. Photoexcitation gives a random distribution of time-evolving defects throughout a crystal. Due to the low concentration of the excited species and the large range of conformations that excited species can sample during relaxation, the coherent diffraction pattern will only contain a partial picture of the excitation process. The diffuse scattering, however, provides access to local structural information that cannot be observed with crystallography [105, 106]. The lack of long-range order that leads to diffuse scattering also makes the scattering significantly weaker than coherent Bragg diffraction. This has made time-resolved applications of diffuse scattering very challenging at synchrotrons. Given that diffuse scattering experiments will greatly benefit from the increased flux of XFELs, and that disordered systems have a dominant presence in chemistry and biology, developing the experimental and theoretical tools necessary for time-resolved diffuse scattering will be among the first developments at XFELs.

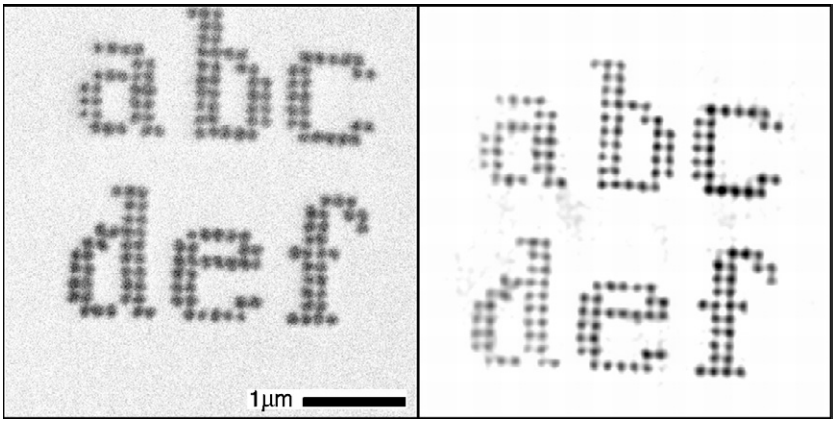

Figure 15. Image reconstruction from a diffuse scattering pattern. Left, a scanning electron micrograph of the sample (gold dots on a SiN membrane). Right, the image reconstructed from the diffraction pattern produced by 1.7 nm soft x-rays. From [108].

8.2. Imaging

X-ray scattering has been the most powerful tool for determining the structure of condensed matter, even of complex macromolecules, at atomic resolution. The only limitations today are the ability to crystallize the object of interest and the radiation damage that disturbs the structure while the scattering data is collected. The classic problem of determining the phase for each Bragg reflection from intensity data has been largely overcome using the anomalous scattering from one or a few atoms in the structures, a technique now widely used at synchrotron sources. There are, however, a significant number of important macromolecules that have not been able to be crystallized, including the general class of membrane proteins. In addition there are cases where radiation damage has also been a significant impediment to achieving atomic resolution.

To overcome both of these problems an idea has emerged [107] to use the extraordinary per-pulse intensity and femtosecond pulse duration from an XFEL to collect diffraction patterns from single biomolecules. This beautiful idea would overcome the issue of crystallization and if it proves feasible, it would also avoid the radiation damage limitation. At the crux of the idea is the ability to obtain the phases from a continuous diffraction pattern of a single object. Sayre recognized some 50 years ago that applying Shannon's ideas would permit one to get the phases from a single unit cell, if one sampled the diffraction pattern at half the Bragg spacing. The extension of this idea to real experiments by Miao *et al* [108] has put the concept of oversampling on a firm basis (see figure 15).

It all sounds simple, but based on the work of Wabnitz *et al* [57] one naturally asks whether the molecule does not undergo a giant Coulomb explosion before the full XFEL pulse has passed the sample. The concept of Hajdu and coworkers requires that the sample remain intact for most if not all of the FEL pulse. They have performed extensive simulations [107], which indicate that for pulses with sufficient flux and short enough duration, the molecules do preserve their structure long enough. Figure 16 shows the damage landscape as a function of photon pulse duration and intensity. It is clear that the pulse duration needs to approach 5 fs to be able to use the full intensity that the FEL can deliver. It is comforting that calculations based on a continuum model of the biomolecule using hydrodynamic codes gives similar

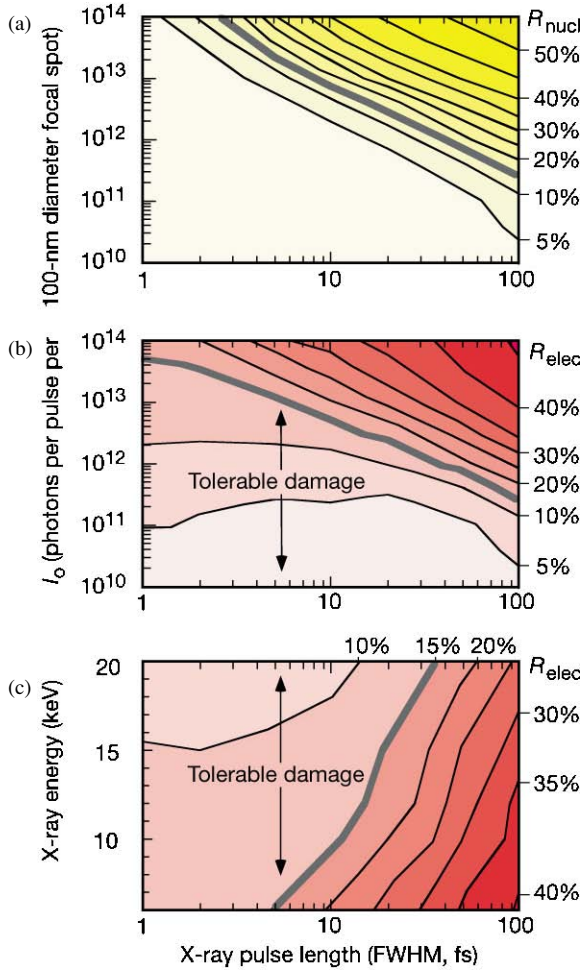

Figure 16. The landscape of radiation damage tolerance. Calculated effects of x-ray pulse intensity, pulse length and photon energy on crystal damage, and the resulting decrease in fidelity of the crystal structure derived from the diffraction pattern. The contour lines plot crystallographic *R* factors. A low *R* factor in this case indicates minimal atomic motion during the time of exposure. From [103].

results for damage thresholds, also indicating that pulses approaching 5 fs will be required if near-atomic-resolution structures are to be obtained.

If one proceeds under the assumption that the pulse duration/intensity issues can be addressed and the molecules will survive, there remain significant questions about inverting the continuous diffraction data with missing information at the smallest angles. This was a problem that Miao *et al* solved by 'filling in' that region with low-resolution optical diffraction data, which permitted their inversion algorithm to converge and retrieve the real-space image of the sample. Recent advances in the development of phase retrieval algorithms have shown that one can invert diffraction data even if the central region is missing. This so-called 'shrink wrap' algorithm defines the boundary between sample and no sample and thus imposes a constraint that permits the phase retrieval to converge [109].

There remains the problem of getting sufficient intensity at the large scattering angles required for near-atomic-scale resolution. Conceptually, this can be solved by simply adding up diffraction patterns from numerous single-molecule data sets. However, is there enough scattered intensity from any single pulse to permit determination of the orientation with sufficient accuracy? Significant progress has recently been made in this area, and results from Elser indicate that it should be possible to classify diffraction patterns with sufficient angular accuracy to perform the necessary averaging [110].

If diffraction imaging at near-atomic-resolution is possible, it will certainly not be confined to the determination of the structures of large biomolecules. Robinson and co-workers have already collected coherent scattering data from single nanocrystals [111]. The reconstructed shapes of these particles have reasonable fidelity, considering the quality of the data. If XFEL imaging proves feasible for such objects, then one can imagine looking at the response of a nanocrystal to a pump laser, and the associated structural dynamics triggered by the impulse. If the laser pulse is of sufficient intensity, one can expect pressure-induced phase changes as well as those triggered by changes in the electronic structure caused by the laser field.

9. Conclusions

Synchrotron radiation has revolutionized the use of x-ray techniques to study atomic and electronic structures in the broadest set of scientific disciplines that could be imagined. They have become an everyday tool. The ability to combine the imaging power of SR with the time resolution available today from optical laser systems will provide a new paradigm for the study of dynamics on the atomic scale. The steady development of accelerator technology, making full use of developments in conventional lasers, has opened the door to the construction of free electron lasers extending to the hard x-ray regime. Already FELs have reached their design goals for wavelengths in the 100 nm range [30, 36] and have produced exciting and unexpected scientific results [57]. The XFEL at SLAC is in an advanced stage of design with first operation expected in 2009, and the European XFEL is not far behind. The potential scientific impact of these sources is immense and the unexpected awaits.

Acknowledgments

We are indebted to Horst Schmidt-Böcking who invited us to contribute this review article. We are well aware that our own contributions to the field are only marginal compared with those of innumerable colleagues over the last 35 years.

References

[1] Milonni P W and Eberly J H 1988 *Lasers* (New York: Wiley Interscience) chapter 13
[2] Brabec T and Krausz F 2000 *Rev. Mod. Phys.* **72** 545
[3] Einstein A 1905 *Ann. Phys.* **17** 132
[4] Einstein A 1905 *Ann. Phys.* **17** 891
[5] Palmer R V 1972 *J. Appl. Phys.* **43** 3014
[6] Robinson K W 1985 *Nucl. Instrum. Methods* A **239** 111
[7] Csonka P 1978 *Part. Acc.* **8** 225
[8] Madey J M J 1971 *J. Appl. Phys.* **42** 1906–13
[9] Elias R E, Fairbank W M, Madey J M J, Schwettman H A and Smith T I 1976 *Phys. Rev. Lett.* **36** 717–20
[10] Deacon D A G, Elias L R, Madey J M J, Ramian G J, Schwettman H A and Smith T I 1977 *Phys. Rev. Lett.* **38** 892
[11] Kondratenko A M and Saldin E L 1980 *Part. Accelerators* **10** 207–16

[12] Murphy J B and Pellegrini C 1985 *Nucl. Instrum. Methods* A **237** 159–67
[13] Pellegrini C 1988 *Nucl. Instrum. Methods* A **272** 364
[14] Fraser J S, Sheffield R L and Gray E R 1986 *Nucl. Instrum. Methods* A **250** 71–6
[15] Carlsten B E 1989 *Nucl. Instrum. Methods* A **285** 313–9
[16] Qiu X, Batchelor K, Ben -Zvi I and Wang X-J 1996 *Phys. Rev. Lett.* **76** 3723–6
[17] Bane K 1987 *AIP Conf. Proc.* **153** 971
[18] Seeman J *et al* 1991 *US Particle Accelerator Conference* IEEE Conf. Proc. 91CH3038-7 p 2064
[19] Seeman J *et al* 1991 *US Particle Accelerator Conference* IEEE Conf. Proc. 91CH3038-7 p 3210
[20] Raubenheimer T 1991 *The Generation and Acceleration of Low Emittance Flat Beams for Future Linear Colliders* SLAC-Report SLAC, Stanford, CA
[21] Cornacchia M *et al* 2001 *A Sub-Picosecond Photon Pulse Facility for SLAC* SCLA-PUB-8950 SLAC, Stanford
[22] Bilderback D H, Elleaume P and Weckert E 2005 *J. Phys. B: At. Mol. Opt. Phys.* **38** S773
[23] Saldin E L, Schneidmiller E A and Yurkov M V 2000 *The Physics of Free Electron Lasers* (Berlin: Springer)
[24] Saldin E L, Schneidmiller E A and Yurkov M V 1999 *Nucl. Instrum. Methods Phys. Res.* A **429** 233–7
[25] Reiche S 2000 *Numerical Studies for a Single Pass High Gain Free-Electron Laser PhD Thesis* Universität Hamburg DESY-Thesis-2000-012
[26] Bonifacio R, Pellegrini C and Narducci L M 1984 *Optics Commun.* **50** 373–8
[27] Hogan M J *et al* 1998 *Phys. Rev. Lett.* **81** 4867–70
[28] Tremaine A *et al* 2002 *Nucl. Instrum. Methods Phys. Res.* A **483** 24–8
[29] Milton S V *et al* 2001 *Science* **292** 2037–41
[30] Ayvazyan V *et al* 2002 *Phys. Rev. Lett.* **88** 104802
[31] *SASE FEL at the TESLA Test Facility, Phase 2* 2002 TESLA-FEL 2002–01 DESY, Hamburg, Germany
[32] Arthur J *et al* 2002 *Linac Coherent Light Source (LCLS) Conceptual Design Report* SLAC-R-593 SLAC, Stanford, USA
[33] Materlik G and Tschentscher T ed 2001 *TESLA Technical Design Report: Part V. The X-Ray Free Electron Laser* DESY 2001-011; ECFA 2001-209
[34] Bonifacio R, Salvo L D, Pierini P, Piovella N and Pellegrini C 1994 *Phys. Rev. Lett.* **73** 70–3
[35] Saldin E L, Schneidmiller E A and Yurkov M V 1998 *Opt. Commun.* **148** 383–403
[36] Ayvazyan V *et al* 2002 *Eur. Phys. J.* D **20** 149–56
[37] Ayvazyan V *et al* 2003 *Nucl. Instrum. Methods Phys. Res.* A **507** 368–72
[38] Saldin E L, Schneidmiller E A and Yurkov M V 2004 *Opt. Commun.* **239** 161–72
[39] Dohlus M, Flöttmann K, Kozlov O S, Limberg T, Piot P, Saldin E L, Schneidmiller E A and Yurkov M V 2004 *Nucl. Instrum. Methods Phys. Res.* A **530** 217–33
[40] Ischebeck R *et al* 2004 *Proc. EPAC 2004 (Lucerne, Switzerland)* pp 2577–9
[41] Richter M *et al* 2003 *Appl. Phys. Lett.* **83** 2970–2
[42] Reininger R, Feldhaus J, Plönjes E, Treusch R, Roper M D, Quinn F M and Bowler M A 2004 *AIP Conf. Proc.* **705** 572–75
[43] Yu L H *et al* 2000 *Science* **289** 932–4
[44] Yu L H *et al* 2003 *Phys. Rev. Lett.* **91** 074801
[45] Li W, Lucchese R R, Doyuran A, Wu Z, Loos H, Hall G E and Suits A G 2004 *Phys. Rev. Lett.* **92** 083002
[46] Saldin E L, Schneidmiller E A and Yurkov M V 2002 *Opt. Commun.* **202** 169–87
[47] Krämer D, Jaeschke E and Eberhardt W 2004 *The BESSY Soft X-Ray Free Electron Laser* BESSY GmbH Berlin, Germany
[48] Feldhaus J, Saldin E L, Schneider J R, Schneidmiller E A and Yurkov M V 1997 *Opt. Commun.* **140** 341–52
[49] Saldin E L, Schneidmiller E A and Yurkov M V 2000 *Nucl. Instrum. Methods* A **445** 178–82
[50] Saldin E L, Schneidmiller E A and Yurkov M V 2002 *Opt. Commun.* **212** 377–90
[51] Schroeder C B, Pellegrini C, Reiche S, Arthur J and Emma P 2002 *Nucl. Instrum. Methods Phys. Res.* A **483** 89–93
[52] Emma P, Bane K, Cornacchia M, Huang Z, Schlarb H, Stupakov G and Walz D 2004 *Phys. Rev. Lett.* **92** 074801
[53] Zholents A A and Fawley W M 2004 *Phys. Rev. Lett.* **92** 224801
[54] Saldin E L, Schneidmiller E A and Yurkov M V 2004 *Opt. Commun.* **237** 153–64
[55] Zholents A A, Fawley W M, Emma P, Huang Z, Stupakov G and Reiche S 2004 *Proc. 26th Int. Free Electron Laser Conference (Trieste, Italy, 29 August–3 September, 2004)*
[56] Krinsky S and Huang Z 2003 *Phys. Rev. ST AB* **6** 050702
[57] Wabnitz H *et al* 2002 *Nature* **420** 482–5
[58] Siedschlag C and Rost J M 2004 *Phys. Rev. Lett.* **93** 043402
[59] Wabnitz H 2004 Private communication

[60] Sobierajski R *et al* 2003 *Proc. 24th Int. Free Electron Laser Conference (Argonne, USA, 9–13 September, 2002)* II77–8
[61] Krzywinski J *et al* 2004 *Proc. 26th Int. Free Electron Laser Conference (Trieste, Italy, 29 August–3 September, 2004)*
[62] Steeg B *et al* 2004 *Appl. Phys. Lett.* **84** 657–9
[63] Hentschel M *et al* 2001 *Nature* **414** 509–13
[64] Shenoy G K and Stöhr J eds 2000 *LCLS—The First Experiments* SLAC-R-611
[65] Zewail A H 2000 *J. Phys. Chem.* A **104** 5660
[66] Harris A L, Brown J K and Harris C B 1988 *Annu. Rev. Phys. Chem.* **39** 341
[67] Maroncelli M, Macinnis J and Fleming G R 1989 *Science* **243** 1674
[68] Barbara P F, Walker G C and Smith T P 1992 *Science* **256** 975
[69] Waldeck D H 1991 *Chem. Rev.* **91** 415
[70] Zewail A H 1988 *Science* **242** 1645
[71] Ho W 1996 *J. Phys. Chem.* **100** 13050
[72] Banin U and Ruhman S 1993 *J. Chem. Phys.* **98** 4391
[73] Walhout P K *et al* 1995 *J. Phys. Chem.* **99** 7568
[74] Genberg L *et al* 1991 *Science* **251** 1051
[75] Lim M, Jackson T A and Anfinrud P A 1995 *Science* **269** 962
[76] Budde F *et al* 1991 *Phys. Rev. Lett.* **66** 3024
[77] Prybyla J A, Tom H W K and Aumiller G D 1992 *Phys. Rev. Lett.* **68** 503
[78] Gaffney K J, Piletic I R and Fayer M D 2002 *J. Phys. Chem.* A **106** 9428
[79] Gaffney K J *et al* 2002 *J. Phys. Chem.* A **106** 12012
[80] Yang H *et al* 2001 *J. Am. Chem. Soc.* **123** 4204
[81] Rothenberger G, Negus D K and Hochstrasser R M 1983 *J. Chem. Phys.* **79** 5360
[82] Velsko S P, Waldeck D H and Fleming G R 1983 *J. Chem. Phys.* **78** 249
[83] Sension R J *et al* 1993 *J. Chem. Phys.* **98** 6291
[84] Mathies R A *et al* 1988 *Science* **240** 777
[85] Dobler J *et al* 1988 *Chem. Phys. Lett.* **144** 215
[86] Song L, Elsayed M A and Lanyi J K 1993 *Science* **261** 891
[87] Song L and El-Sayed M A 1998 *J. Am. Chem. Soc.* **120** 8889
[88] Mathies R A *et al* 1991 *Ann. Rev. Biophys. Biophys. Chem.* **20** 491
[89] Hasson K C, Gai F and Anfinrud P A 1996 *Proc. Natl. Acad. Sci. USA* **93** 15124
[90] Gai F *et al* 1998 *Science* **279** 1886
[91] Kobayashi T, Saito T and Ohtani H 2001 *Nature* **414** 531
[92] Herbst J, Heyne K and Diller R 2002 *Science* **297** 822
[93] Miller A D *et al* 2002 *Science* **297** 1163
[94] Ge N H *et al* 1998 *Science* **279** 202
[95] Martini I, Barthel E and Schwartz B 2001 *Science* **293** 462
[96] Lehr J *et al Science* **284** 635
[97] Srinvivasan R, Lobastov V, Ruanthis C Y and Zewail A 2003 *Helv. Chim. Acta* **86** 1763
[98] Srajer V, Teng T Y, Ursby T, Pradervand C, Ren Z, Adachi S, Schildkamp W, Bourgeois D, Wulff M and Moffat K 1996 *Science* **274** 1726–9
[99] Perman B *et al* 1998 *Science* **279** 1946–50
[100] Moffat K 2001 *Chem. Rev.* **101** 1569–81
[101] Schotte F, Lim M, Jackson T, Smirnov A, Soman J, Olson J, Phillips G, Wulff M and Anfinrud P 2003 *Science* **300** 1944–7
[102] Schmidt V, Pahl R, Srajer V, Anderson S, Ren Z, Ihee H, Rajagopal S and Moffat K 2004 *Proc. Natl. Acad. Sci. USA* **101** 4799–8004
[103] Techert S and Zachariasse K A 2004 *J. Am. Chem. Soc.* **126** 5593–6000
[104] Techert S, Schotte F and Wulff M 2001 *Phys. Rev. Lett.* **86** 2030–3
[105] Szöke A 1999 *Chem. Phys. Lett.* **313** 777–9
[106] Sondhauss P and Wark J S 2003 *Acta Crytallogr.* A **59** 7–13
[107] Neutze R *et al* 2000 *Nature* **406** 752–7
[108] Miao J *et al* 1999 *Nature* **400** 342–4
[109] Marchesini S *et al* 2003 *Phys. Rev.* B **68** 140101(R)
[110] Elser V unpublished
[111] Williams G J *et al* 2003 *Phys. Rev. Lett.* **90** 175501